Palm NMR and 1-Chip NMR

Nan Sun, *Member, IEEE*, Tae-Jong Yoon, Hakho Lee, William Andress, Ralph Weissleder, and Donhee Ham, *Member, IEEE*

***Abstract*—In our earlier work, we developed a 2-kg NMR system, which was 60× lighter, 40× smaller, yet 60× more spin-mass sensitive than a 120-kg state-of-the-art commercial benchtop system. Here we report on two new nuclear magnetic resonance (NMR) systems that represent further orders-of-magnitude size reduction and lab-on-a-chip capability. The first system, which weighs 0.1 kg and can be held in the palm of a hand, is the smallest NMR system ever built, and is 1200× lighter, 1200× smaller, yet 150× more spin-mass sensitive than the commercial system. It is enabled by combining the physics of NMR with a CMOS RF transceiver. The second system, which even integrates a sample coil, directly interfaces the CMOS chip with a sample for lab-on-a-chip operation. The two systems detect biological objects such as avidin, human chorionic gonadotropin, and human bladder cancer cells.**

***Index Terms*—Biosensors, CMOS, radio-frequency integrated circuits(RFICs), lab on a chip, nuclear magnetic resonance (NMR).**

I. Introduction

PARTICULAR types of atomic nuclei, such as protons in hydrogen atoms, act like tiny bar magnets due to their spin. Nuclear magnetic resonance (NMR) is a resonant interaction between a radio-frequency (RF) magnetic field and the nucleic magnets placed in a static magnetic field. Since the detailed resonance behavior is influenced by the environment of the nucleic magnets, NMR can be used to examine properties of a material, thus, it has a wide array of applications in technology and science, such as biomolecular sensing, medical imaging, and oil detection, to name a few.

The benefits of NMR would be broadly available, if NMR instruments can be made small, thus, at low cost. For example, a miniature NMR biosensor may enable disease screening in doctor's office at an affordable cost. Nonetheless, NMR systems remain bulky, heavy, and expensive, with their use limited in hospitals, testing facilities, and laboratories. A case in point is the state-of-the-art commercial benchtop NMR system of [3], which weighs approximately 120 kg.

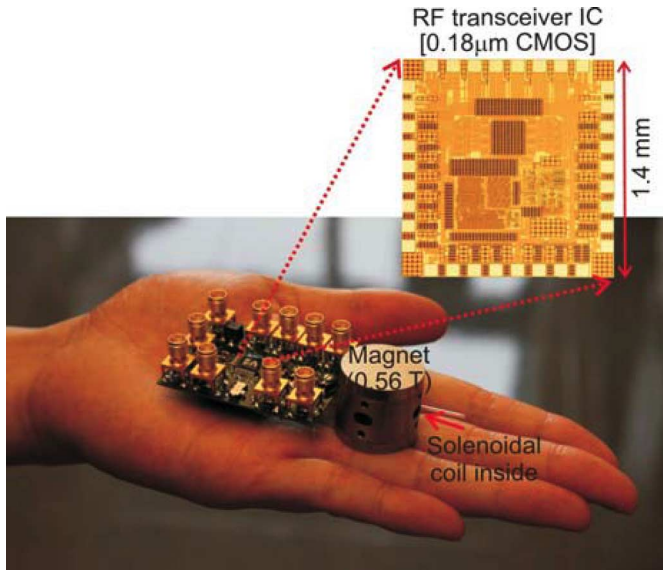

Fig. 1. 0.1-kg palm NMR system.

The large size is attributed to the following reason. An NMR system consists of a magnet to produce a static magnetic field, a sample coil, and an RF transceiver to generate an RF magnetic field and to monitor the resonance. Since a larger-sized magnet tends to yield a stronger NMR signal even for the same static field strength and hence relaxes the sensitivity requirement on the transceiver design, large magnets are used, leading to the bulky size, where the magnet is by far the largest component.

In our prior work [1], [2], we developed a 2-kg *portable NMR system*, which was 60× lighter, 40× smaller, yet 60× more spin-mass sensitive than the 120-kg commercial system [3]. To achieve this miniaturization, we took an approach opposite to the convention: we opted to use a small magnet the size of a hamburger[1] (this magnet and the magnet of the commercial system both produce the static field of ∼0.5 T), and to detect the NMR signal weakened by the small-sized magnet, we developed a partially integrated, high-performance CMOS RF transceiver and a separate high-quality planar coil.

The present paper reports on two new NMR systems, which represent yet another orders-of-magnitude size reduction and lab-on-a-chip capability.

First, we report a 0.1-kg *palm NMR system* (Fig. 1), the smallest complete NMR system to our best knowledge. It

Manuscript received April 21, 2010; revised July 19, 2010; accepted July 28, 2010. Date of publication October 18, 2010; date of current version December 27, 2010. This paper was approved by Guest Editor Alison Burdett. This work was supported by the Harvard Nanoscale Science and Engineering Center under Grant NSF/PHY 06-46094, and in part by the World Class University program through National Research Foundation of Korea funded by the Ministry of Education, Science, and Technology (R31-2008-000-10100-0).

N. Sun was with the School of Engineering and Applied Sciences, Harvard University, Cambridge, MA 02138 USA. He is now with the Department of Electrical and Computer Engineering, University of Texas at Austin, Austin,TX 78712 USA (e-mail: nansun@seas.harvard.edu).

T.-J. Yoon, H. Lee, and R. Weissleder are with the Center for Systems Biology, Massachusetts General Hospital, Harvard Medical School, Boston, MA 02114 USA.

W. Andress and D. Ham are with the School of Engineering and Applied Sciences, Harvard University, Cambridge, MA 02138 USA (e-mail: donhee@seas.harvard.edu).

Color versions of one or more of the figures in this paper are available online at http://ieeexplore.ieee.org.

Digital Object Identifier 10.1109/JSSC.2010.2074630

[1]As this hamburger-sized magnet will reappear in this paper, we mention its dimension here. It is of a cylindrical shape, with height 5.5 cm and base diameter 8.0 cm, and weighs 1.25 kg.

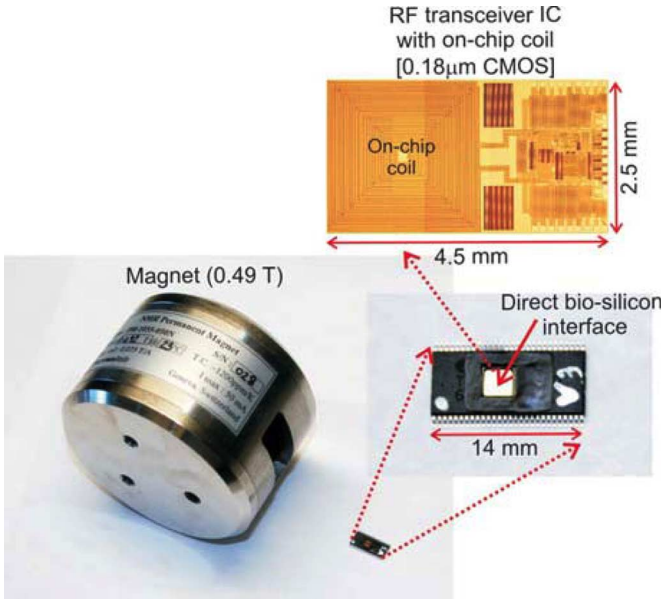

Fig. 2. 1-chip NMR system with lab-on-a-chip capability.

is 1200× lighter, 1200× smaller, yet 150× more spin-mass sensitive than the 120-kg commercial system [3]. As compared to our prior 2-kg portable NMR system [1], [2], the palm system is 20× lighter, 30× smaller, and yet 2.5× more spin-mass sensitive. To attain this further substantial size/cost reduction, we use a tiny magnet only the size of a ping-pong ball (∼0.56 T) (Fig. 1).[2] This considerably lowers the NMR signal, which we overcome by designing a new, high performance CMOS RF transceiver. As the signal is already lowered by the ping-pong-ball-sized magnet, the palm system uses a high-quality solenoidal coil, not to further weaken the signal.

Second, we report a *1-chip NMR system* (Fig. 2). Even the NMR coil is integrated as a planar spiral in the CMOS chip along with the transceiver developed for the palm system. The transceiver's performance permits the use of the lossy on-chip coil that lowers the signal-to-noise ratio. Not to further weaken the signal-to-noise ratio, the 1-chip system operates with the hamburger-size magnet of our prior work [1], [2]. Due to this magnet, the weight reduction from our prior work [1], [2] is by 25%, but the point of the 1-chip system is lab-on-a-chip operation. For example, a biological sample can be placed directly on the coil of the chip for on-chip screening of disease markers. The chip can be disposable for one-time diagnostic testing. The direct interface may also enable oil detection [4] and quantum computing [5] on a CMOS chip. The 1-chip system has the same spin-mass sensitivity as our prior work [1], [2], while 60 times more spin-mass sensitive than the commercial system [3].

The key to these two developments is the new CMOS RF transceiver, an advance from the transceiver of our prior work [1], [2]. First, the new transceiver achieves the sensitivity to cope with the signal-to-noise ratio lowered by the ping-pong-ball-size magnet (palm system) or the lossy on-chip coil (1-chip system). Second, the new transceiver attains the highest level of integration among existing NMR transceivers. Our prior work [1], [2] did not integrate a power amplifier (PA), as meeting the large power tuning requirement of NMR was not trivial with an integrated PA. We integrate a PA in the new transceiver by devising a power tuning scheme that exploits atomic nuclei's natural high-Q ($\sim 10^4$) filtering ability.

Another highlight of this work is NMR-based biomolecular sensing relevant to disease screening. We detect not only avidin proteins, but also human chorionic gonadotropin (hCG) protein, which is a cancer marker for male patients for cancers such as choriocarcinoma, germ cell tumor, and islet cell tumor. At the cell level, we detect human bladder cancer cells.

This work was briefly presented in the 2010 *IEEE ISSCC* [6]. Here we seek its full exposure. Sections II and III present the design and measurements of the CMOS RF transceiver. Section IV reports NMR experiments and NMR-based biomolecular sensing. Section V compares the palm and 1-chip systems with other NMR miniaturization efforts. We refer readers unfamiliar with NMR to our earlier publication [2] for quick introduction to the NMR basics.

II. CMOS NMR RF Transceiver IC Design

A. Overall Architecture and Operation

Fig. 3(a) and (b) shows the architectures of the NMR RF transceivers in the palm and 1-chip systems, respectively. The palm system [Fig. 3(a)] uses an off-chip solenoidal coil; the 1-chip system [Fig. 3(b)] employs an on-chip planar spiral coil. The dashed lines in the figures indicate CMOS integration boundaries for the two systems. The transceiver architecture is essentially the same between the two systems, but the transceiver-coil matching networks are different for a reason explained in Section II-D, thus, the two separate figures were prepared to avoid confusion. The electrical characteristics of the coils will be described in Section II-B.

All NMR experiments in our work, including biomolecular sensing, are done with protons in hydrogen atoms in aqueous samples. In the palm system, a sample is placed inside the solenoidal coil and is subjected to a static magnetic field $B_0 \sim 0.56\,\mathrm{T}$ produced by the ping-pong-ball-sized magnet. In the 1-chip system, a sample placed on the planar coil is subjected to a static magnetic field $B_0 \sim 0.49\,\mathrm{T}$ produced by the hamburger-sized magnet. The NMR frequency for protons subjected to B_0 is given by $\omega_0/2\pi \approx 42.6 \cdot B_0$ MHz [2]: 23.9 MHz for the palm system; 20.9 MHz for the 1-chip system.

In the excitation phase of NMR, switches **S1** and **S2** are closed, and the transmitter [upper half of Fig. 3(a) or (b)] sends in an RF current to the coil to produce an RF magnetic field in the sample. If the RF magnetic field's frequency is tuned into the NMR frequency, ω_0, it resonantly excites the protons, increasing their energy. During this excitation phase, the receiver amplifier stages [in the lower half of Fig. 3(a) or (b)], except the front-end stage, are isolated from the large excitation signal by short-circuiting their inputs and open-circuiting the RF signal path, using switches **S3** through **S11** controlled by the **ENA** command signal. The front-end stage remains connected to the large excitation signal, in order not to place switches in front

[2]This ping-pong-ball-sized magnet has a cylindrical shape, whose height and base diameter are 2.3 and 2.5 cm, respectively. It weighs 0.07 kg.

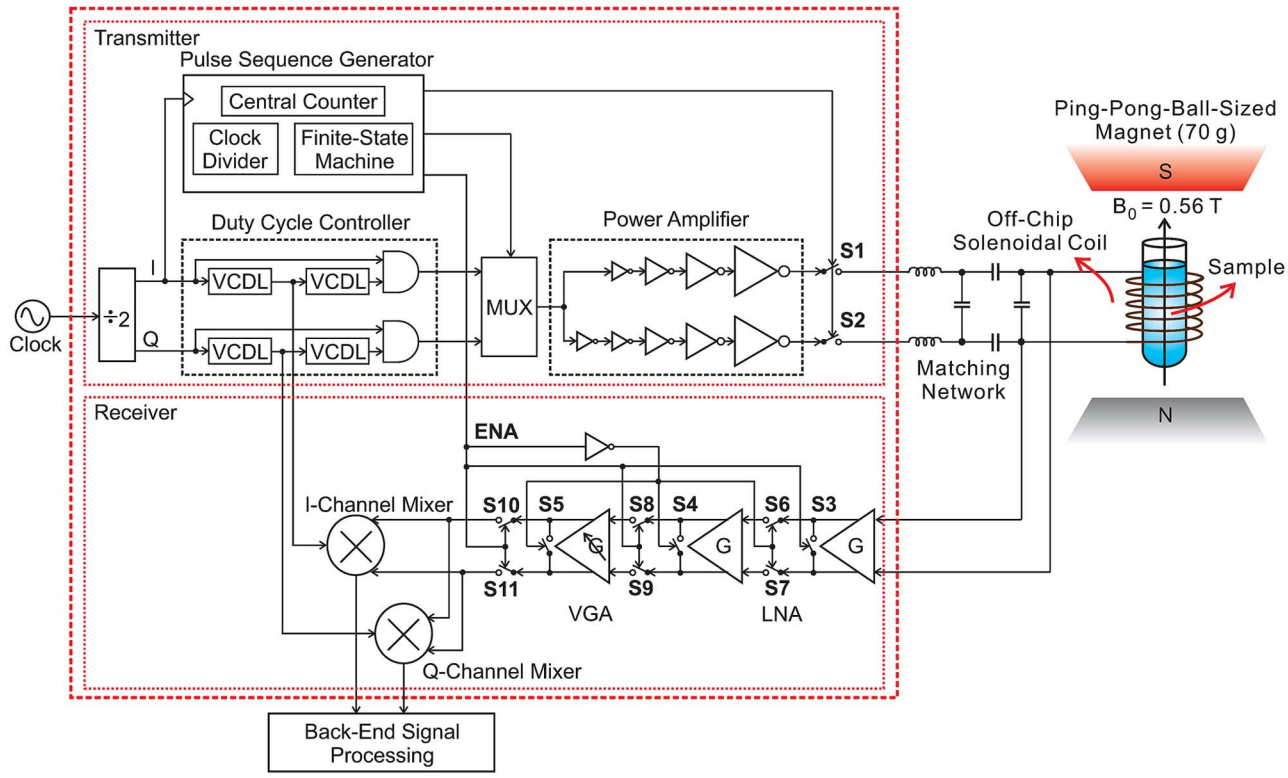

Fig. 3. CMOS RF transceiver architecture. (a) CMOS NMR RF transceiver architecture for the palm system. (b) CMOS NMR RF transceiver architecture for the 1-chip system.

of it, as lossy switches at the front end would compromise the receiver noise figure.

After protons acquire sufficient energy, the RF transmission is ceased by turning off switches **S1** and **S2**. Nearly simulta-

neously, the receiver path [lower half of Fig. 3(a) or (b)] is activated by operating switches **S3** through **S11** in the configuration that is opposite their configuration during the excitation phase. In this reception phase of NMR, the excited protons electromagnetically interact with the coil, inducing an AC voltage signal with the NMR frequency, ω_0, across the coil. This NMR signal, whose peak-to-peak voltage is on the order of 100 nV and bandwidth is about 1 kHz, is amplified and frequency-down-converted by the heterodyne receiver. The intermediate frequency (IF) for the receiver is set at 3 kHz, which is high enough to mitigate $1/f$ noise, and low enough to facilitate the rejection of out-of-band noise by placing an off-chip band pass filter at the outputs of the mixers. Two mixers are used to perform the frequency down-conversion with quadrature oscillator outputs. The outputs of the mixers, after the band-pass filtering, are digitized by an off-chip analog-to-digital converter, and subsequently undergo an image rejection signal processing, to avoid the extra 3-dB noise figure degradation brought by the frequency down-conversion.

NMR transceivers usually employ two separate clocks, one with the NMR frequency for the proton excitation, and the other as the local oscillator with the frequency different than the NMR frequency by the target IF to produce the correct IF. In contrast, in our transceiver, both the transmitter excitation signal and the receiver local oscillator signal share the identical frequency, both derived from the same clock (Fig. 3). In this scheme the clock frequency is set at a value 3 kHz larger than the NMR frequency so as to produce the target IF of 3 kHz. Therefore the excitation signal is 3 kHz off from the NMR frequency. Nonetheless, it can still excite protons, for it has a nonzero bandwidth due to its finite duration and the bandwidth can be made large enough to cover ω_0. The advantage of this single-clock scheme, which we adopt from our prior work [1], [2], is simplicity: we only need to tune one frequency in the NMR experiment, instead of tuning two clock frequencies while maintaining their difference at 3 kHz.

B. Characteristics of the Coils

The off-chip solenoidal coil of the palm system [Figs. 1 and 3(a)] has 14 turns around a capillary tube (inner diameter: 0.75 mm; outer diameter: 1 mm). The sample volume inside the coil is 2 μL. The coil has an inductance of 100 nH, a resistance of 0.5 Ω, and a Q of 28, all measured at the NMR frequency 23.9 MHz of the palm system.

The on-chip planar spiral coil of the 1-chip system [Figs. 2 and 3(b)] has 25 turns, and occupies an area of 2.5 mm $\times$ 2.5 mm. We use a package that exposes the coil part while encapsulating the rest of the chip (Fig. 2). The open part of the package above the coil can hold a 5 μL of sample. To reduce the coil resistance, 5 metal layers are connected in parallel. SONNET EM field solver is used in the coil design. The coil has an inductance of 430 nH, a resistance of 31 Ω, and a Q of 1.9, all measured at the NMR frequency 20.9 MHz of the 1-chip system. The low Q is due mainly to the coil's dc resistance, while the substrate and skin effect are less pronounced at the NMR frequency.

C. Transmitter With Proton Filter

The power amplifier (PA) of the NMR transmitter in general needs to have a large output power tuning capability in order to control the amount of energy that goes into the protons during the NMR excitation phase. Our prior work of [1], [2] did not integrate a PA, since meeting the power tuning requirement was not trivial with an integrated PA. The transmitter in the present work, which is shown in detail in Fig. 4, integrates the entire front-end transmitter chain, including a PA. We manage to tune the PA's output power by exploiting the proton's natural high-Q ($\sim 10^4$) filtering ability. The transmitter hence is one important circuit aspect of the present work.

To start with, the PA is realized as a differential chain of cascaded four inverter stages (Fig. 4, bottom right). The inverters are consecutively quadrupled in size to sequentially amplify power and ensure drivability at the output. This class-D arrangement is simple to design and does not consume static power, but it produces a square wave output with a fixed voltage amplitude of $V_{\rm DD}$, thus, calling for a technique to tune its output power.

To this end, we tune the duty cycle of the transmitted signal. A given transmitted square wave (frequency[3]: ω_0; amplitude: $V_{\rm DD}$) with a specific duty cycle (Fig. 4, top) assumes a particular power distribution of the fundamental tone at ω_0 and higher harmonics. The power distribution over the harmonics varies with the duty cycle. Here we only need to look at the variation of the power at ω_0 with the duty cycle, for higher harmonics lie outside the 'proton filter' band: protons are a high-Q ($\sim 10^4$) band-pass filter centered at ω_0, in the sense that they are not excited by signals that lie outside the frequency band. As the duty cycle is altered from 0% to 50%, the ω_0-component changes its voltage from 0 to $(4/\pi)V_{\rm DD}$ (Fig. 4, top right). This effectively corresponds to the output power tuning.

The duty cycle is tuned by the duty cycle controller that consists of cascaded voltage-controlled delay lines (VCDL) and AND gates (Fig. 4, bottom left). Both of its quadrature square-wave inputs, $I_{\rm in}$ and $Q_{\rm in}$ (frequency: ω_0; amplitude $V_{\rm DD}$), have a 50% duty cycle. The AND operation on $I_{\rm in}$ and its delayed version yields $I_{\rm out}$, whose duty cycle varies with the amount of the total delay. The same principle applies to $Q_{\rm in}$ and $Q_{\rm out}$. As the total delay changes from 0 to π/ω_0, the duty cycle shifts from 50% to 0%.

This duty-cycle-tuning scheme ensures that regardless of the total delay, $I_{\rm out}$ and $Q_{\rm out}$ are always maintained in quadrature phase, which is required to execute the CPMG NMR excitation pulse-sequence technique [7], which we use. As can be seen in the timing diagram of Fig. 5, the rising (and falling) edges of $I_{\rm out}$ and $Q_{\rm out}$ are separated by a quarter of the period. The CPMG pulse-sequence technique also requires that the LO signal for the I-channel mixer be in phase with $I_{\rm out}$ and the LO signal for the Q-channel mixer be in phase with $Q_{\rm out}$. This requirement can be readily satisfied by using $I_{\rm mid}$ and $Q_{\rm mid}$ of Fig. 4 as the two LO signals, as the fundamental tones of $I_{\rm mid}$ and $Q_{\rm mid}$ are always in phase with the fundamental tones of $I_{\rm out}$

[3]As mentioned in Section II-A, the actual frequency is 3 kHz larger than the NMR frequency, but for simplicity without altering essence, we do not include the extra 3 kHz here.

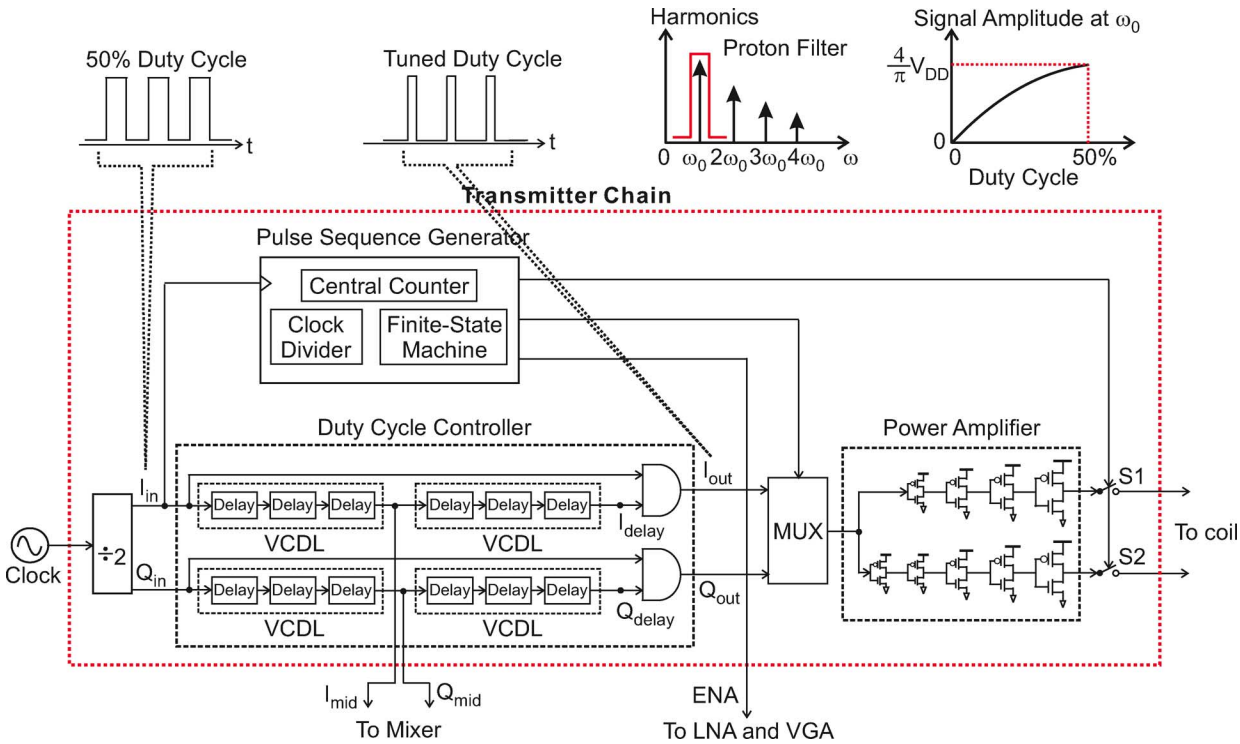

Fig. 4. Transmitter chain and power tuning scheme.

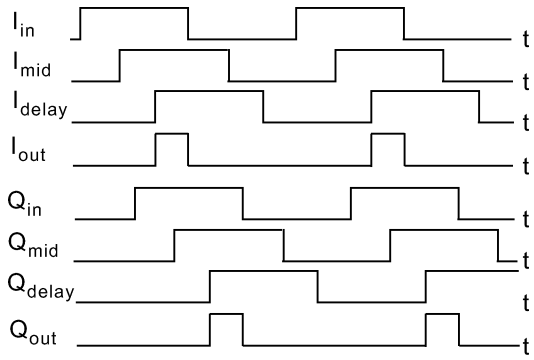

Fig. 5. Timing diagram and phase relationship of duty cycle tuning.

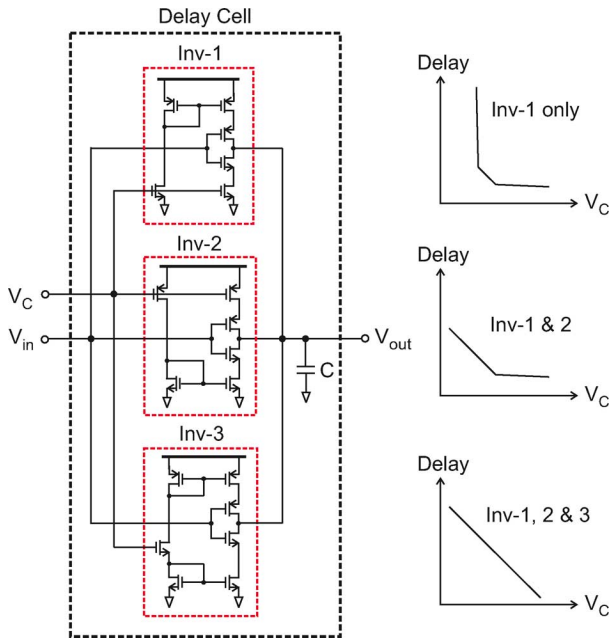

Fig. 6. Schematic of a single delay cell.

and Q_{out}, respectively, regardless of the total amount of delay, as seen in the timing diagram.

Each voltage-controlled delay line in the duty cycle controller consists of 3 voltage-controlled delay cells, and each voltage-controlled delay cell consists of 3 voltage-controlled inverters in parallel (Fig. 6). Inv-1 is a standard current starved inverter. Its delay is not linear with control voltage V_C: with V_C below a certain threshold, the delay tends toward infinity; with large V_C, the delay hardly tunes. Inv-2, a complementary current-starved inverter with a size smaller than Inv-2, prevents the steep delay increase for small V_C. Inv-3, a current-starved inverter with V_C fed after a source follower, sustains a delay reduction with increasing V_C. These combine together to yield a more linear tuning characteristics.

The digital pulse sequence generator (Fig. 4, upper left) controls the MUX and switches **S1** and **S2** to produce an adequate NMR excitation pulse sequence such as the CPMG pulse sequence, an essential task in practical NMR works [7]. The pulse sequence generator also sets the timing scheme for the receiver by controlling switches **S3** through **S11** (see also Fig. 3) in the way explained in Section II-A.

D. Heterodyne Receiver With Passive Amplification

While the transmitter is a substantial design/integration-level advance from our prior work [1], [2], the heterodyne receiver,

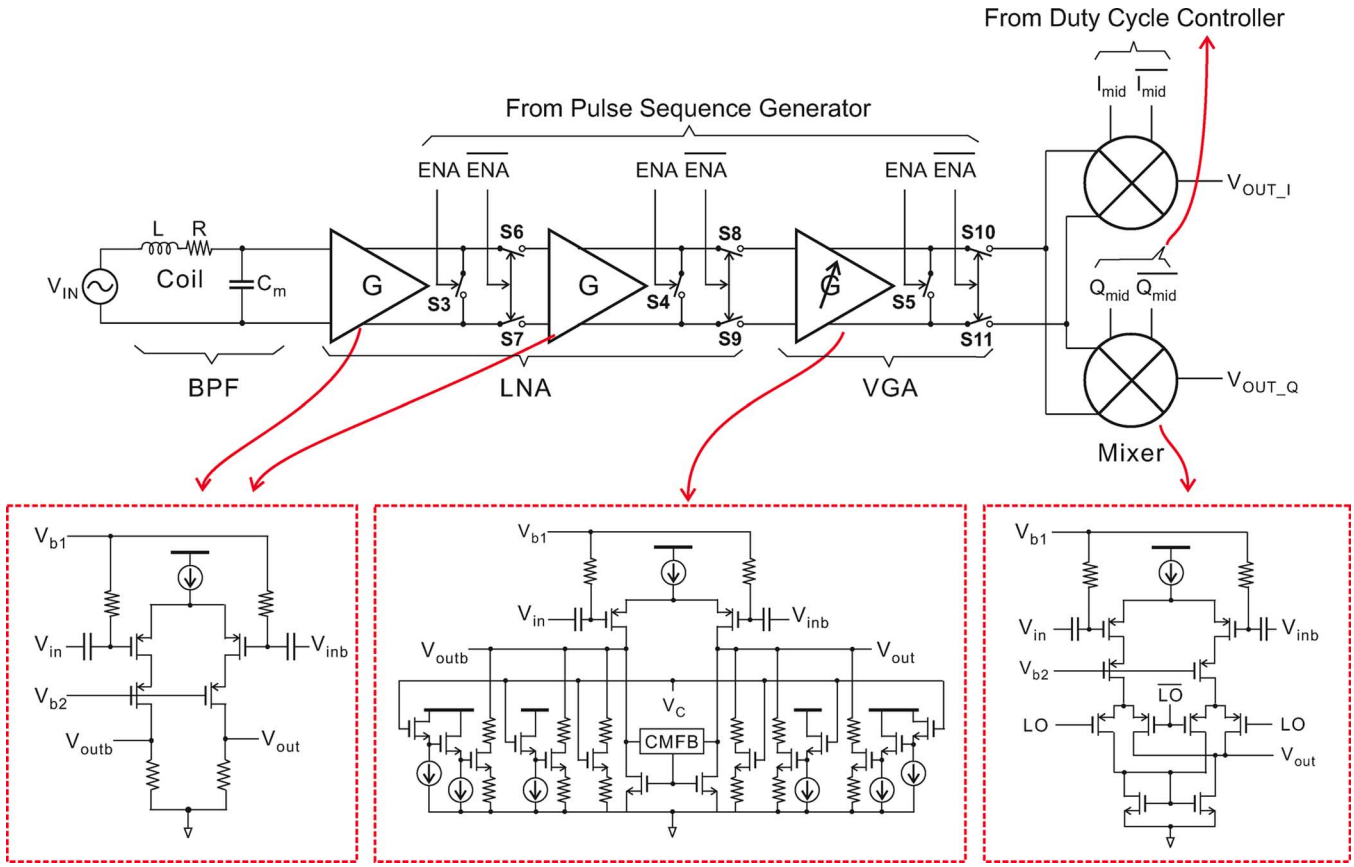

Fig. 7. Receiver chain.

shown in details in Fig. 7, is a detailed revision of the prior work for performance improvement. The receiver consists of a low noise amplifier (LNA), a variable gain amplifier (VGA), two mixers, and switches **S3** through **S11**, whose usage was explained in Section II-A. To handle the NMR signal-to-noise ratio substantially weakened by the ping-pong-ball-sized magnet in the palm system or the lossy on-chip coil in the 1-chip system, the noise figure (NF) of the receiver should be minimized. To this end, both minimization of the LNA's input referred noise and optimum LNA-coil noise matching are necessary.

To minimize the LNA's input referred noise, we take the following measures in our new LNA design: 1) resistive loads are used in place of active loads. This obviates the need for a common-mode feedback circuit, thus, reducing the noise sources. To compensate for the low gain due to the passive loads, we use a two-stage amplifier; 2) PMOS transistors are used as input devices to minimize $1/f$ noise and substrate coupling from digital circuits; and 3) the cascode configuration attenuates coupling between the local oscillator and the LNA.

For the optimum LNA-coil noise matching, we place a capacitor C_m in parallel with the coil (Fig. 7, left), where C_m resonates with the coil inductance L at the NMR frequency, ω_0. This LC network forms a band-pass filter. The magnitude of its frequency response, illustrated in Fig. 8,[4] peaks at ω_0. The filter may be viewed as a preamplifier with "passive" voltage gain of $\sqrt{Q^2+1}$, where Q is the coil quality. As C_m has negligible loss compared to the coil, the passive amplification hardly adds any noise and maintains the original signal-to-noise-ratio (SNR) from the coil. In other words, the passive amplifier has an NF close to 0 dB but with the gain of $\sqrt{Q^2+1}$, which leads to a low receiver NF according to the Friis equation [8]. While this passive amplification scheme is not applicable for wideband signals due to the frequency-dependent transfer function (Fig. 8), it suits well the NMR signal, which in general has a very narrow bandwidth (∼1 kHz in our case). Nonetheless, non-optimal coil-LNA impedance matching at 50 Ω, instead of the optimum noise matching based on the passive amplification, has been a conventional choice, as the former is convenient in the conventional NMR electronics that has largely been realized at the discrete level. This shows an advantage of the integrated NMR electronics.

The LNA-coil resonance matching for minimum noise figure corresponds to an impedance mismatch between the LNA and the coil. In contrast, the PA and the coil need to be impedance-matched for maximum power delivery. In order to simultaneously achieve both the optimum LNA-coil noise matching and PA-coil power matching, the palm system adopts an advanced matching network we devised in our prior work [2] [Fig. 3(a), right]. In the 1-chip system, on the other hand, we provide only the LNA-coil resonance matching using C_m [Fig. 3(b), right] without using the advanced network, thus, the PA and the coil are not impedance matched. This is because the components

[4]Since the LNA's input impedance is much larger than that of the coil and C_m at $\omega_0/2\pi$ (∼20 MHz), we may ignore the effect of the LNA.

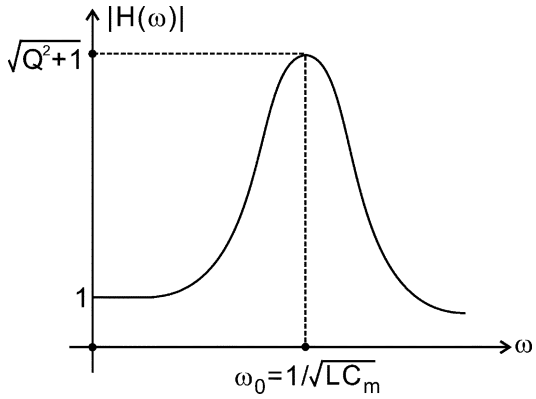

Fig. 8. Magnitude of the frequency response of the LC passive amplifier.

of the advanced network are too large to be integrated, and using discrete components defeats the purpose of constructing a 1-chip system. Nonetheless, the 1-chip system manages to deliver a reasonable amount of power to the coil for proton excitation.

The VGA (Fig. 7) is to handle both the palm and 1-chip systems, whose NMR signal strengths are different. The mixer is a double-balanced Gilbert mixer with an active load. Both the VGA and the mixer share the same schematics as those in our prior work [1], [2].

III. Transceiver Measurements

We implemented two variations of the NMR RF transceiver with essentially the same architecture [Fig. 3(a) and (b)], one for the palm system and the other for the 1-chip system, in 0.18-μm CMOS technology. The transceiver IC for the palm system occupies an area of 1.4 mm $\times$ 1.4 mm (Fig. 1), and is packaged in a 32 lead QFP package. The transceiver IC with the on-chip planar coil for the 1-chip system occupies an area of 4.5 mm $\times$ 2.5 mm (Fig. 2), and is so packaged in a 56 lead TSSOP package that the coil part of the chip, on which an aqueous sample is placed, is left exposed while the rest of the chip is encapsulated.

A. Receiver Measurements

To measure the receiver input-referred noise, we feed a $-$100-dBm, 21-MHz RF signal to the receiver's LNA input, and use a 21.003-MHz square wave as an LO. From the signal and noise power spectrum measured at the receiver's mixer output (Fig. 9) using an Agilent E4448 spectrum analyzer, the receiver gain is inferred, and then, by dividing the measured output noise with the gain, the receiver input referred noise of 1.26 nV/$\sqrt{\text{Hz}}$ is extracted. In this process, the image effect due to the frequency down-conversion is factored out, for the actual operation indeed performs image rejection via back-end digital signal processing (Section II-A).

Using the measured input referred noise and the coil impedance (Section II-B), we infer the receiver NF. In the palm system, a passive gain of 28 offered by the resonance matching (Section II-D) lowers the NF from 22.5 dB to 0.9 dB. In the 1-chip system, a passive gain of 2.1 lowers the NF from 6.1 dB to 2.2 dB. The combination of the small input referred noise and the resonance matching (optimum noise matching) leads

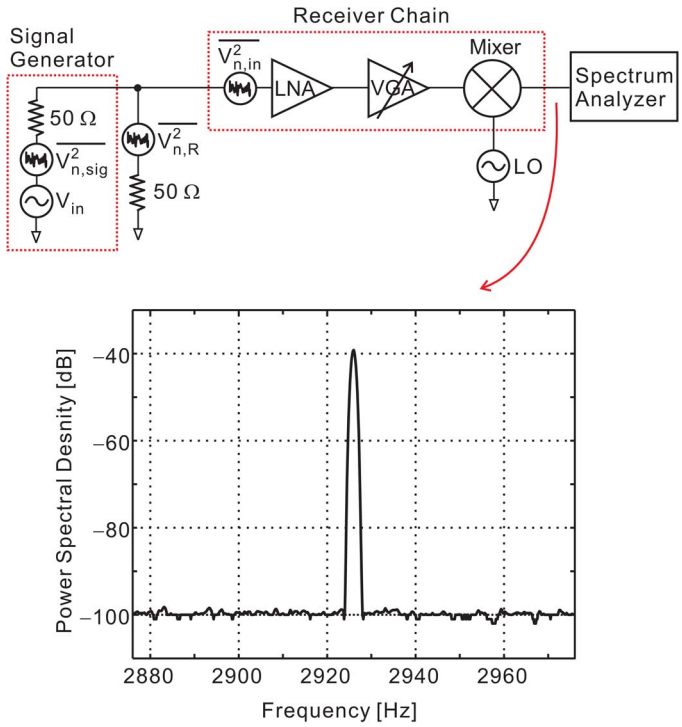

Fig. 9. Measured receiver output power spectrum for a $-$100-dBm, 21-MHz RF signal and with a 21.003-MHz square wave LO.

to sufficiently low NF, making the ping-pong-ball-size magnet and the lossy on-chip coil viable system options.

B. Transmitter Measurements

The measured output impedance of the differential PA (Section II-C) is 27 Ω. With V_{DD} of 3.3 V, the maximum deliverable power at the fundamental tone is 82 mW.

The measured delay versus control voltage, V_C, of the entire voltage-controlled delay line (VCDL) in the duty cycle controller (Fig. 4, bottom left) is shown in Fig. 10. The delay is altered from 29 ns to 2 ns, as V_C is varied from 0 to 3.3 V.

The measured duty cycle as a function of V_C for a 21-MHz excitation signal is shown in Fig. 11. As V_C is changed from 0 to 3.3 V, the duty cycle increases from 0% to 45%. This translates to the tuning of output power at the fundamental tone from 0 to 80 mW (98% of the total deliverable power of 82 mW).

The performance of the transceivers are summarized in Table I.

IV. NMR Experiments and NMR-Based Biomolecular Sensing

A. Proton NMR Experiments

NMR is performed on protons of hydrogen atoms in a 2-μL water sample using the palm system. Fig. 12 shows a measured, down-converted NMR signal. The repeated ringings, which are the result of the proton excitations using a CPMG pulse sequence [7], constitute the NMR signal. It decays with characteristic time called T_2, one of the key parameters in NMR experiments [2], which we use in our NMR-based biomolecular sensing, as seen shortly. $T_2 = 100$ ms is extracted from the exponentially decaying envelope of the NMR signal, shown

TABLE I
TRANSCEIVER PERFORMANCE SUMMARY

	Transceiver, Palm system	Transceiver, 1-chip system
Process	0.18-μm CMOS	
Chip area	1.4×1.4 mm^2	4.5×2.5 mm^2
Receiver input referred noise	1.26 nV/$\sqrt{\text{Hz}}$	
Receiver noise figure	0.9 dB	2.2 dB
Transmitter output impedance	27 Ω	
Transmitted signal's duty-cycle range	0% to 45%	
Transmitter available power range	0 to 80 mW	

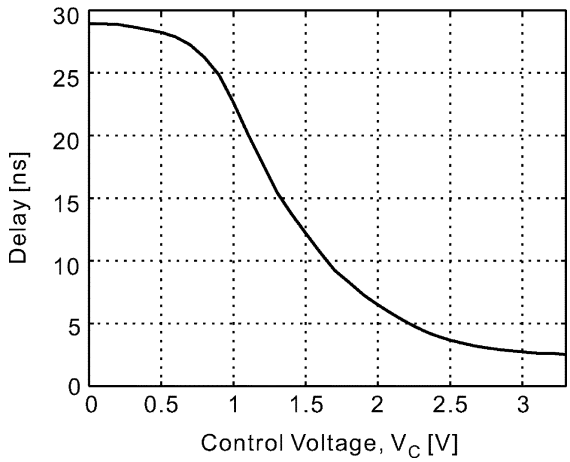

Fig. 10. Measured total VCDL delay versus control voltage, V_C.

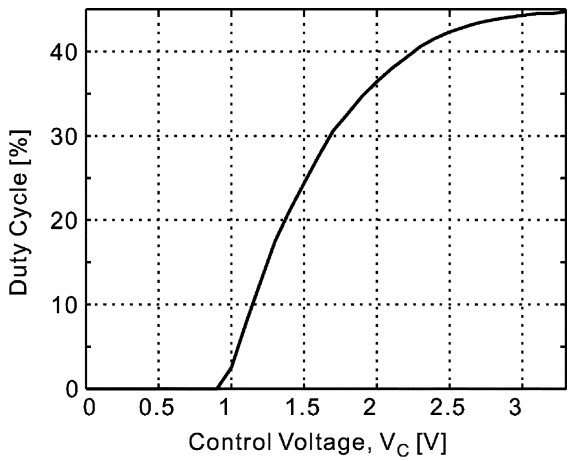

Fig. 11. Measured excitation signal duty cycle versus control voltage, V_C.

as a dotted line. The repeated spikes between the ringings are due to the coupling of the large excitation signals, but they do not compromise the observation of the NMR signal (ringings), as they occur at different time instances. The spin-mass sensitivity[5] is 2.5 times higher than that of our prior work [1], [2], and 150 times higher than that of the state-of-the-art commercial system [3].

Fig. 13(a) shows a measured, down-converted NMR signal obtained in a proton NMR experiment (5-μL water sample) done with the 1-chip system, from which we obtain

[5]The minimum mass of water that produces a detectable NMR signal; a smaller minimum mass corresponds to a higher spin-mass sensitivity.

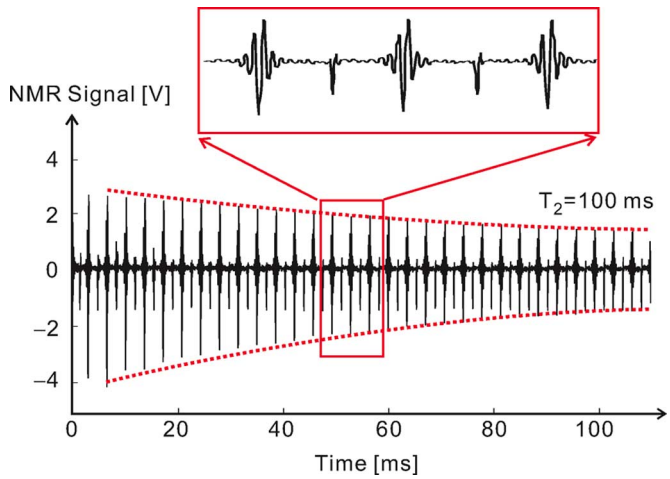

Fig. 12. Water proton NMR signal measured with the palm system.

$T_2 = 722$ ms. The spikes coupled from the large excitation signals are more pronounced, but once again, they do not hamper the observation of the NMR signal due to their occurrence at different time instances. Note the difference between the T_2 values measured using the 1-chip and palm systems. While $T_2 = 722$ ms obtained with the 1-chip system well approximates the true value, $T_2 = 100$ ms obtained with the palm system is a substantial underestimation of the true value, which is due to the pronounced static magnetic field inhomogeneity of the ping-pong-ball sized magnet used in the palm system [7]. Nonetheless, this is not a fundamental problem, as repetition of the CPMG pulses at a faster rate, which the current implementation has no provision for but is easy to incorporate, can readily yield the correct T_2 value [7]. Moreover, in our T_2-based biomolecular sensing experiments that will be presented shortly, we focus on the relative measure of T_2 values.

Fig. 13(b) shows a measured, down-converted NMR signal obtained in another water proton NMR experiment using the 1-chip system, this time, after 0.05 mM magnetic nanoparticles [Fe] (30 nm) are added in the water sample. The measured T_2 is decreased to 93 ms. This reduction of the T_2 value in the presence of magnetic nanoparticles which perturb the NMR behavior is expected from the NMR theory [9].

B. NMR-Based Biomolecular Sensing

Fig. 14 shows the detection of avidin protein using the palm system. Magnetic particles (38 nm) coated with biotins are put into a 2-μL water inside the solenoidal coil. In the absence of

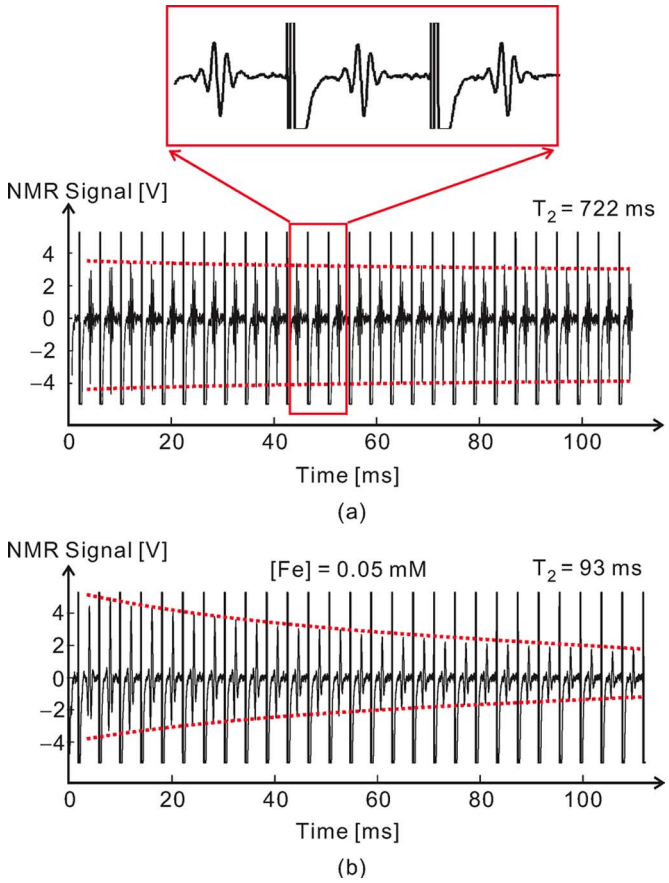

Fig. 13. Measured proton NMR signal with the 1-chip system. (a) Water. (b) Water with magnetic nanoparticles (0.05 mM).

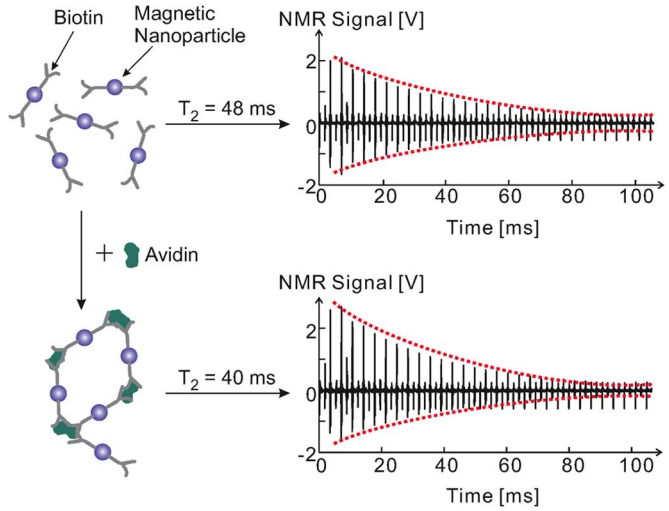

Fig. 14. Avidin detection using biotinylated magnetic particles with the palm system.

avidin (Fig. 14, top), the particles stay monodispersed, yielding T_2 of 48 ms. In the presence of avidin (Fig. 14, bottom), the biotinylated magnetic particles bind to avidin to self-assemble into clusters [10]. The effectively larger magnetic particles reduce T_2 to 40 ms [10]. The reduction in T_2 corresponds to the detection of avidin. The palm system detects down to 1 avidin molecule in 600 million water molecules.

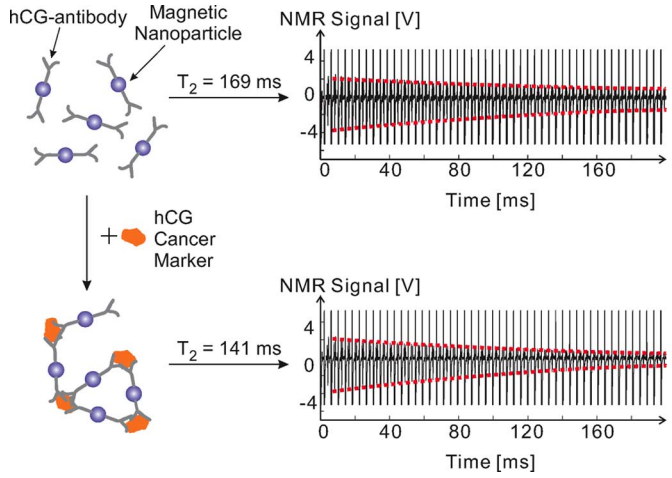

Fig. 15. hCG detection with the 1-chip system.

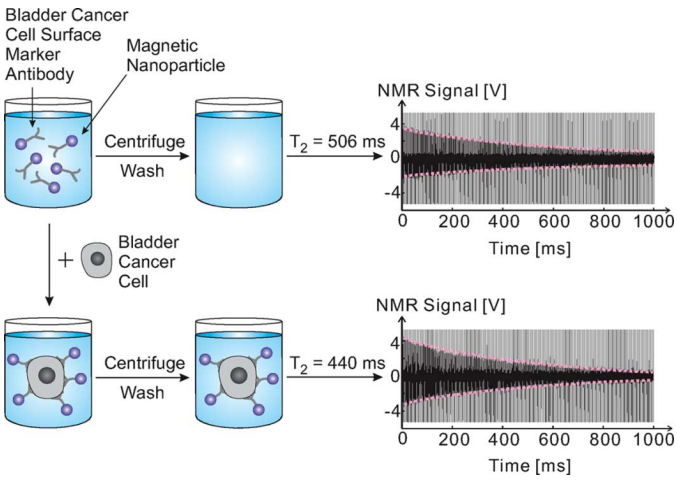

Fig. 16. Human bladder cancer cell detection with the 1-chip system.

We use the 1-chip system to detect human chorionic gonadotropin (hCG), the hormonal protein found in blood or urine (Fig. 15). Its primary use for female patients is as a pregnancy indicator, but for male patients it serves as a marker for certain cancers, such as choriocarcinoma, germ cell tumors, and islet cell tumors. Magnetic particles (38 nm) coated with mouse monoclonal antibody to hCG are put into a 5-μL water sample placed on the on-chip planar coil. $T_2 = 169$ ms in the absence of hCG, and $T_2 = 141$ ms in its presence, which corresponds to the detection of hCG. The 1-chip system detects down to 1 hCG molecule in 12 billion water molecules.

We also detect human bladder cancer cells using the 1-chip system (Fig. 16). Magnetic particles (40 nm) coated with monoclonal antibody to bladder cancer cell surface markers are put into a 5-μL water sample placed on the on-chip coil. In the absence of the cancer cells, the magnetic particles are mono-dispersed (Fig. 16, top left); in the presence of the cancer cells, magnetic particles bind to the cell surface (Fig. 16, bottom left). A following centrifugation step [11] separates the cells and unbounded magnetic particles in different layers, and then the unbounded magnetic particles are washed out. As a result, for the sample without cancer cells, all magnetic particles are removed in the wash-out process, leading to a longer T_2 of 506 ms

TABLE II
NMR SYSTEM MINIATURIZATION EFFORTS

	Transceiver integration	Small magnet	On-chip coil
This work: palm NMR	◯ Receiver; transmitter.	◯ 0.07 kg	×
This work: 1-chip NMR	◯ Receiver; transmitter.	◯ 1.25 kg	◯
[12]	×	◯ 1.25 kg	×
[13]	×	◯ 2.5 kg	×
[14]	◯ Receiver	×	◯
[15]	◯ LNA	×	◯
[16]	◯ LNA	×	×
[17]	◯ LNA; PA	×	×
[18]	◯ LNA	×	×

(Fig. 16, top); for the sample with cancer cells, the magnetic particles that bind to the cell surface remain, leading to a shorter T_2 of 440 ms (Fig. 16, bottom). The reduction in T_2 indicates the existence of cancer cells. The concentration detection threshold is 17.5 cells per μL.

V. COMPARISON TO OTHER MINIATURIZATION WORKS

Before concluding, we compare our palm and 1-chip systems to other NMR system miniaturization efforts in Table II. The advance from our prior work [1], [2] and the state-of-the-art commercial benchtop system [3] was elaborated in Section I, so they do not enter the table. As seen in the table, other works [12]–[18] use small magnets [12], [13], or integrated transceivers [14]–[18], but not both as we did. In addition, the integrated transceivers used in [14]–[18] have integration levels considerably lower than the palm and 1-chip system. Overall, in terms of the entire system dimension and integration level, the palm and 1-chip systems represent a meaningful advance from the previous miniaturization efforts.

VI. CONCLUSION

By combining the physics of NMR with CMOS RF integrated circuits, we developed two miniature NMR systems (palm NMR system and 1-chip NMR system), which represent orders-of-magnitude size reduction and lab-on-a-chip capabilities. Using these systems, we performed biomolecular sensing ultimately aimed at disease screening. We would like to view the value of this work from a few different angles. First, NMR has a broad array of applications in addition to biomolecular sensing, and from this general NMR point of view, our work on the small, low-cost NMR is a meaningful development that can help make the benefits of NMR closer to our lives. Second, from the circuit point of view, our work showcases how CMOS RF integrated circuits can be used not only for wireless applications, but also in one day for human health care and disease screening in direct interface with biological systems. Third, from the biotechnology point of view, our work suggests a way to perform general-purpose disease screening in the low-cost, hand-held platform.

ACKNOWLEDGMENT

The authors thank T2 Biosystems Inc., Cambridge, MA, for purchasing the magnet used in the palm system, and Dr. Pablo Prado and Dr. Vasiliki Demas for the related technical assistance with the magnet. The authors thank Dr. Demas also for winding the solenoidal coil used in the palm system, and Dr. Yong Liu of the IBM T. J. Watson Research Center, Yorktown Heights, NY, for suggestions.

REFERENCES

[1] Y. Liu, N. Sun, H. Lee, R. Weissleder, and D. Ham, "CMOS mini nuclear magnetic resonance system and its application for biomolecular sensing," in *IEEE Int. Solid-State Circuits Conf. Dig. Tech. Papers*, Feb. 2008, pp. 140–141.

[2] N. Sun, Y. Liu, H. Lee, R. Weissleder, and D. Ham, "CMOS RF biosensor utilizing nuclear magnetic resonance," *IEEE J. Solid-State Circuits*, vol. 44, no. 5, pp. 1629–1643, May 2009.

[3] Bruker Optics. The Minispec TD-NMR Analyzers. Bruker Optics, Billerica, MA. [Online]. Available: http://www.brukeroptics.com/minispec.html

[4] B. Sun and K.-J. Dunn, "A global inversion method for multi-dimensional NMR logging," *J. Magn. Reson.*, vol. 172, pp. 152–160, Jan. 2005.

[5] L. M. K. Vandersypen, M. Steffen, G. Breytal, C. S. Yannoni, M. H. Sherwood, and I. L. Chuang, "Experimental realization of Shor's quantum factoring algorithm using nuclear magnetic resonance," *Nature*, vol. 414, pp. 883–887, Dec. 2001.

[6] N. Sun, T.-J. Yoon, H. Lee, W. Andress, V. Demas, P. Prado, R. Weissleder, and D. Ham, "Palm NMR and one-chip NMR," in *IEEE Int. Solid-State Circuits Conf. Dig. Tech. Papers*, Feb. 2010, pp. 488–489.

[7] C. P. Slichter, *Principles of Magnetic Resonance*. New York: Springer-Verlag, 1992.

[8] T. H. Lee, *The Design of CMOS Radio-Frequency Integrated Circuits*. Cambridge, U.K.: Cambridge Univ. Press, 1998.

[9] A. Roch, R. N. Muller, and P. Gillis, "Theory of proton relaxation induced by superparamagnetic particles," *J. Chem. Phys.*, vol. 110, no. 11, pp. 5403–5411, Mar. 1999.

[10] J. M. Perez, L. Josephson, T. O'Loughlin, D. Hoegeman, and R. Weissleder, "Magnetic relaxation switches capable of sensing molecular interactions," *Nature Biotechnol.*, vol. 20, pp. 816–820, Aug. 2002.

[11] H. Lee, T.-J. Yoon, J.-L. Figueiredo, F. K. Swirski, and R. Weissleder, "Rapid detection and profiling of cancer cells in fine-needle aspirates," *Proc. Nat. Acad. Sci.*, vol. 106, no. 30, pp. 12459–12464, Jul. 2009.

[12] H. Lee, E. Sun, D. Ham, and R. Weissleder, "Chip-NMR biosensor for detection and molecular analysis of cells," *Nature Med.*, vol. 14, no. 8, pp. 869–874, Aug. 2008.

[13] G. Eidmann, R. Savelsberg, P. Blümler, and B. Blümich, "The NMR mouse, a mobile universal surface explorer," *J. Magn. Reson.*, ser. A, vol. 122, pp. 104–109, 1996.

[14] G. Boero, J. Frounchi, B. Furrer, P.-A. Besse, and R. S. Popovic, "Fully integrated probe for proton nuclear magnetic resonance magnetometry," *Rev. Sci. Instrum.*, vol. 72, pp. 2764–2768, Jun. 2001.

[15] J. Anders, G. Chiaramonte, P. SanGiorgio, and G. Boero, "A single-chip array of NMR receivers," *J. Magn. Reson.*, vol. 201, pp. 239–249, Dec. 2009.

[16] T. Cherifi, N. Abouchi, G.-N. Lu, L. Bouchet-Fakri, L. Quiquerez, B. Sorli, J.-F. Chateaux, M. Pitaval, and P. Morin, "A CMOS microcoil-associated preamplifier for NMR spectroscopy," *IEEE Trans. Circirts Syst. I, Reg. Papers*, vol. 52, no. 12, pp. 2576–2583, Dec. 2005.

[17] L.-S. Fan, S. Hsu, J.-D. Jin, C.-V. Hsieh, W.-C. Lin, H. Hao, H.-L. Cheng, K.-C. Hsueh, and C.-Z. Lee, "Miniaturization of magnetic resonance microsystem components for 3D cell imaging," in *IEEE Int. Solid-State Circuits Conf. Dig. Tech. Papers*, Feb. 2007, pp. 166–167.

[18] R. L. Magin, A. G. Webb, and T. L. Peck, "Miniature magnetic resonance machines," *IEEE Spectrum*, vol. 34, no. 10, p. 51, Oct. 1997.

Nan Sun (S'06–M'11) received the B.S. degree in electronic science and technology from Tsinghua University, Beijing, China, in 2006, where he ranked top first in the Department of Electronic Engineering and graduated with the highest honor and the Outstanding Undergraduate Thesis Award. He received the Ph.D. degree in engineering science from the School of Engineering and Applied Sciences, Harvard University, Cambridge, MA, in 2010. His Ph.D. research examined two independent subjects. First, he developed several CMOS RF biomolecular sensors utilizing nuclear magnetic resonance (NMR) to pursue disease screening in low-cost hand-held platforms. The miniature NMR systems can be used not only for medical diagnostics, but also for petroleum exploration, high-precision magnetometry, and quantum computing. Second, he developed several digital background calibration techniques for pipelined analog-to-digital converters (ADCs) for their low-power design.

He is currently an Assistant Professor in the Department of Electrical and Computer Engineering, University of Texas at Austin. The current intellectual focus of his research is on: 1) micro- and nanoscale solid-state platforms (silicon ICs and beyond) as an electrical, electrochemical, and optical analytical tool for biotechnology and medicine; 2) low-cost medical imaging systems; 3) miniature spin resonance systems; and 4) analog, mixed-signal, and RF integrated circuits.

Dr. Sun received the First-Class Outstanding Student Award from Tsinghua University each year from 2003 to 2006. He won the Top Prize in the Intercollegiate Physics Competition in 2003. He is the recipient of a Samsung Fellowship, Hewlett Packard Fellowship, and Analog Devices Outstanding Student Designer Award in 2003, 2006, and 2007, respectively. He won the Harvard Teaching Award in three consecutive years from 2008 to 2010.

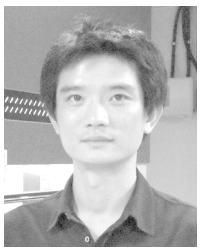

Tae-Jong Yoon is a Postdoctoral Scholar at the Center for Systems Biology, Massachusetts General Hospital, Harvard Medical School, Boston, MA. He received the Ph.D. degree in chemistry from Seoul National University, South Korea, in 2006, where he studied the synthesis and surface modification of magnetic and fluorescent nanomaterials aimed at biological applications under Prof. Jin-kyu Lee.

His current research is on labeling bacteria, cancer cells, or proteins with magnetic nanoparticles and their detection using diagnostic magnetic resonance technology with Prof. Ralph Weissleder.

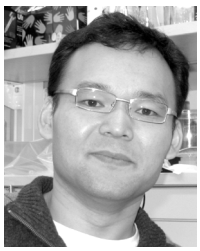

Hakho Lee is an Instructor in the Biomedical Engineering program at the Center for Systems Biology, Massachusetts General Hospital and Harvard Medical School, Boston, MA. He received the Ph.D. degree in physics from Harvard University, Cambridge, MA, in 2005, and joined the Center for Molecular Imaging Research at the Massachusetts General Hospital, Harvard Medical School, as a Research Associate. For his Ph.D. work, he implemented a new type of micro-total-analysis-systems by combining integrated circuits and microfluidics; as a Research Associate at the Massachusetts General Hospital, he developed the diagnostic magnetic resonance (DMR) technology based on miniature nuclear magnetic resonance instruments and magnetic nanoparticles. With Prof. Ralph Weissleder, he is leading the clinical translation of the DMR technology for cancer diagnosis and prognosis. His research group focuses on developing new multifunctional nanomaterials and biomedical sensors.

William Andress received the B.S. degree (highest honors) in electrical engineering and computer science from Harvard University, Cambridge, MA, in 2004, where he is currently working toward the Ph.D. degree in electrical engineering and applied physics. His Ph.D. research examines collective behaviors of electrons and their quantum effects in low-dimensional solid-state nanoscale devices including semiconductor quantum wires and carbon nanotubes, and on their applications for ultrafast electronics.

Mr. Andress was awarded the Thomas T. Hoopes Prize for best senior thesis. He is a recipient of the Analog Devices Outstanding Student Designer Award and the National Defense Science and Engineering Graduate Fellowship.

Ralph Weissleder is currently a Professor at Harvard Medical School, Director of the Center for Systems Biology at Massachusetts General Hospital (MGH), Boston, MA, and Attending Clinician (Interventional Radiology) at MGH. He is also a member of the Dana Farber Harvard Cancer Center, an Associate Member of the Broad Institute (Chemical Biology Program), and a member of the Harvard Stem Cell Institute (HSCI) leading its Imaging Program. His research interests include the development of novel molecular imaging techniques, tools for detection of early disease detection, development of nanomaterials for sensing, and systems analysis. His research has been translational, and several of his developments have led to advanced clinical trials with anticipated major impacts when these methods become routinely available. He is currently the Principal Investigator of several RO1 NIH grants, a P50 Center grant, a U24 grant, and a UO1 consortium focusing on nanotechnology. He has published over 500 original publications in peer-reviewed journals and has authored several textbooks.

Dr. Weissleder is a founding member of the Society for Molecular Imaging Research and served as its President in 2002. His work has been honored with numerous awards including the J. Taylor International Prize in Medicine, the Millennium Pharmaceuticals Innovator Award, the AUR Memorial Award, the ARRS President's Award, the Society for Molecular Imaging Lifetime Achievement Award, the Academy of Molecular Imaging 2006 Distinguished Basic Scientist Award, and the 2008 RSNA Outstanding Researcher Award. He is an elected member of the U.S. National Academies Institute of Medicine (2009).

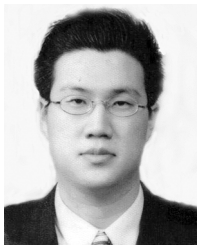

Donhee Ham (S'99–M'02) received the B.S. degree in physics from Seoul National University, Seoul, Korea, in 1996, where he graduated *summa cum laude* with the Valedictorian Prize as well as the Presidential Prize, ranked top first across the Natural Science College, and also with the Physics Gold Medal (sole winner). Following a year and a half of mandatory military service in the Korean Army, he went to the California Institute of Technology for graduate training in physics. There he worked on general relativity and gravitational astrophysics under Barry Barish, and later received the Ph.D. degree in electrical engineering in 2002, winning the Charles Wilts Prize, given for the best thesis in electrical engineering. His doctoral work examined the statistical physics of electrical circuits.

He is currently the Gordon McKay Professor of Applied Physics and Electrical Engineering at Harvard University, Cambridge, MA, where he has been with School of Engineering and Applied Sciences since 2002. His work experience includes the Caltech-MIT Laser Interferometer Gravitational Wave Observatory (LIGO), IBM T. J. Watson Research, Visiting Professorship at Postech, Korea, IEEE conference technical program committees including the IEEE International Solid-State Circuits Conference and the IEEE Asian Solid-State Circuits Conference, advisory board for the IEEE International Symposium on Circuits and Systems (ISCAS), international advisory board for the Institute for Nanodevice and Biosystems, and various U.S., Korea, and Japan industry, government, and academic technical advisory positions on subjects including ultrafast electronics, science and technology at the nanoscale, and the convergence of biotechnology and information technology. He served as a Guest Editor for the IEEE JOURNAL OF SOLID-STATE CIRCUITS and was a coeditor of *CMOS Biotechnology* (Springer, 2007). The intellectual focus of his research laboratory at Harvard University is on: 1) electronic, electrochemical, and optical analysis of biological systems on solid-state chips for biotechnology and medicine; 2) quantum plasmonic circuits using 1–D nanoscale devices; 3) spin-based quantum computing; 4) stochastic, nonlinear, and quantum dynamics; and 5) RF, analog, and mixed-signal integrated circuits.

Dr. Ham was the recipient of the IBM Doctoral Fellowship, Caltech Li Ming Scholarship, IBM Faculty Partnership Award, IBM Research Design Challenge Award, Silver Medal in the National Mathematics Olympiad, Korea Foundation of Advanced Studies Fellowship, and Harvard's Hoopes prize (shared with William F. Andress). He was recognized by the MIT Technology Review as among the world's top 35 young innovators in 2008 (TR35), for his group's work on a CMOS RF biomolecular sensor using nuclear spin resonance to pursue disease screening in a low-cost, handheld platform. He holds an honorary degree from Harvard University.